

CHAPTER 83

A NUMERICAL MODEL OF NEARSHORE CURRENTS DUE TO IRREGULAR WAVES

Masataka Yamaguchi*

ABSTRACT

This paper presents a numerical model of nearshore currents due to irregular waves. The radiation stress is estimated by a current-depth refraction model for irregular waves, in which the energy dissipation due to wave breaking is modeled through the use of a saturated frequency spectrum in shallow water. The model is in reasonable agreement with measured wave height, mean water level variation and observed nearshore current patterns. Next, the model is applied to the computation of wave transformation and nearshore currents on a uniformly sloping beach and on model topographies with complicated contour lines. Comparison with the results based on a regular wave model shows that wave irregularity has a smoothing effect on cross-shore distributions of wave height, mean water level variation and longshore currents, but that it does not have much effect on nearshore current patterns.

1. INTRODUCTION

In most nearshore current models, a regular wave theory including finite amplitude wave theory (Yamaguchi, 1986) has been used for the calculation of wave transformation in shoaling water and in the surf zone, and the resulting radiation stress which is a driving force of nearshore currents. Since ocean waves are irregular waves approximated by the superposition of many component waves with different frequency and direction, a nearshore current model taking into account the effect of wave irregularity is needed for better understanding and description of coastal phenomena. Nevertheless, it seems that there are no numerical models of nearshore currents due to irregular waves applicable to an arbitrary bottom topography, although analytical models of longshore currents by Collins(1972), Battjes(1972) and Thornton & Guza (1986) and a numerical model of longshore

* Prof., Dept. of Ocean Eng., Ehime Univ., Bunkyocho 3, Matsuyama 790, Ehime Pref., Japan

currents by Hubertz (1984), are available. Therefore, the aim of this study is to present a numerical model of near-shore currents due to irregular waves, in which wave transformation is computed by a current-depth refraction model, and to establish its applicability by comparison with the results of experiments and observations of wave transformation and nearshore currents. Then, based on the numerical computations, the effect of wave irregularity on them and the characteristics of nearshore currents on two-dimensional model topographies are discussed.

2. MODEL DESCRIPTION

(1) Wave transformation model

The wave transformation model is to solve the conservation equation of wave action spectral density ($w = E(k_x, k_y) / \sigma_m$) and the equations for wave number components (k_x, k_y) simultaneously, where $E(k_x, k_y)$ is the wave number spectrum and σ_m the relative angular frequency. The former is written as

$$\frac{\partial w}{\partial t} + \frac{dx}{dt} \frac{\partial w}{\partial x} + \frac{dy}{dt} \frac{\partial w}{\partial y} + \frac{dk_x}{dt} \frac{\partial w}{\partial k_x} + \frac{dk_y}{dt} \frac{\partial w}{\partial k_y} = 0 \quad (1)$$

and the latter is

$$\begin{aligned} \frac{\partial k_x}{\partial t} + (C_g \cos \theta + U) \frac{\partial k_x}{\partial x} + (C_g \sin \theta + V) \frac{\partial k_x}{\partial y} \\ = -\frac{gk^3 \operatorname{sech}^2 kD}{2\sigma_m} \frac{\partial D}{\partial x} - k_x \frac{\partial U}{\partial x} - k_y \frac{\partial V}{\partial x} \\ \frac{\partial k_y}{\partial t} + (C_g \cos \theta + U) \frac{\partial k_y}{\partial x} + (C_g \sin \theta + V) \frac{\partial k_y}{\partial y} \\ = -\frac{gk^3 \operatorname{sech}^2 kD}{2\sigma_m} \frac{\partial D}{\partial y} - k_x \frac{\partial U}{\partial y} - k_y \frac{\partial V}{\partial y} \end{aligned} \quad (2)$$

where C_g is the group velocity of the component wave, θ the wave direction, k the wave number, $D (= h + \eta)$ the total water depth including the mean water level variation η , h the still water depth and (U, V) are the wave-induced nearshore current components.

These equations mean that the wave action spectral density in a nondissipative system is conserved along the characteristics defined by

$$\frac{dx}{dt} = C_g \cos \theta + U, \quad \frac{dy}{dt} = C_g \sin \theta + V \quad (3)$$

where the wave number components are computed from

$$\begin{aligned} \frac{dk_x}{dt} &= -\frac{gk^3 \operatorname{sech}^2 kD}{2\sigma_m} \frac{\partial D}{\partial x} - k_x \frac{\partial U}{\partial x} - k_y \frac{\partial V}{\partial x} \\ \frac{dk_y}{dt} &= -\frac{gk^3 \operatorname{sech}^2 kD}{2\sigma_m} \frac{\partial D}{\partial y} - k_x \frac{\partial U}{\partial y} - k_y \frac{\partial V}{\partial y} \end{aligned} \quad (4)$$

Thus, the conservation of the wave action spectral density expressed in frequency-direction space is written as

$$w(f, \theta) = (C_g + U \cos \theta + V \sin \theta) E(f, \theta) / (2\pi k \sigma_m) = \text{const} \quad (5)$$

and is rewritten in the following equation

$$E_2(f_2, \theta_2) = \left\{ \frac{(C_{\sigma 1} + U_1 \cos \theta_1 + V_1 \sin \theta_1) / (k_1 \sigma_{m1})}{(C_{\sigma 2} + U_2 \cos \theta_2 + V_2 \sin \theta_2) / (k_2 \sigma_{m2})} \right\} E_1(f_1, \theta_1) \quad (6)$$

where f is the absolute frequency, $E(f, \theta)$ is the directional spectrum and subscripts '1' and '2' denote the variables at different positions. This is the basic relationship used to compute the transformation of directional spectra. The model can estimate the effects of not only depth-refraction and wave shoaling, but also current refraction.

The energy dissipation due to wave breaking is modeled through the use of a saturated frequency spectrum proposed by Kitaigorodskii et al. (1975)

$$E_{\infty}(f) = \alpha g^2 (2\pi)^{-4} f^{-3} \phi(\omega_h) \quad (7)$$

$$\phi(\omega_h) = \alpha^{-1} (1 + 2\omega_h^2 x / \sinh 2\omega_h^2 x)^{-1}, \quad \omega_h^2 = \sigma_n^2 D / g, \quad x = gk / \sigma_n^2$$

where α is the equilibrium constant at the high frequency tail and g the acceleration of gravity. Assuming the invariability of angular distribution in directional spectra associated with wave breaking, directional spectra including the effect of depth-controlled wave breaking are re-evaluated by

$$E_{new}(f, \theta) = E_{old}(f, \theta) E_{\infty}(f) / E_{old}(f) \quad (8)$$

where directional spectra with subscripts 'new' and 'old' mean directional spectra before and after the inclusion of the wave breaking effect respectively.

The radiation stress components (S_{xx} , S_{xy} , S_{yy}) and wave statistics are obtained by the numerical integration of directional spectra with respect to wave direction and frequency using

$$\begin{aligned} S_{xx} &= \int_0^{\infty} \int_0^{2\pi} \rho g \{n \cos^2 \theta + (n-1/2)\} E(f, \theta) d\theta df \\ S_{xy} = S_{yx} &= \int_0^{\infty} \int_0^{2\pi} \rho g n \cos \theta \sin \theta E(f, \theta) d\theta df \\ S_{yy} &= \int_0^{\infty} \int_0^{2\pi} \rho g \{n \sin^2 \theta + (n-1/2)\} E(f, \theta) d\theta df \end{aligned} \quad (9)$$

and

$$\begin{aligned} E(f) &= \int_0^{2\pi} E(f, \theta) d\theta, \quad m_0 = \int_0^{\infty} E(f) df, \quad m_1 = \int_0^{\infty} f E(f) df, \quad m_2 = \int_0^{\infty} f^2 E(f) df \\ H_{1/3} &= 4.00 \sqrt{m_0}, \quad T_{1/3} = 1.20 \sqrt{m_0 / m_2}, \quad H_{rms} = 2.83 \sqrt{m_0}, \quad T_{m01} = m_0 / m_1 \end{aligned} \quad (10)$$

$$\bar{\theta} = \tan^{-1} \left\{ \int_0^{\infty} \int_0^{2\pi} E(f, \theta) \cos \theta d\theta df \middle/ \int_0^{\infty} \int_0^{2\pi} E(f, \theta) \sin \theta d\theta df \right\}$$

where $n = C_g / C$, C is the wave celerity of the component wave, ρ the density of fluid, m_n the spectral moment, $E(f)$ the frequency spectrum, $H_{1/3}$ the significant wave height, $T_{1/3}$ the significant wave period, H_{rms} the root mean square wave height, T_{m01} the mean wave period and $\bar{\theta}$ the mean wave direction.

The input directional spectrum at the offshore boundary is given by the Bretschneider-Mitsuyasu-type frequency spec-

tral model with $\cos^{2S}(\theta/2)$ type angular distribution function

$$E(f, \theta) = E(f) \cdot D(f, \theta)$$

$$E(f) = 0.257 (H_{1/3})_0^2 (T_{1/3})_0 (T_{1/3})_0 f^{-5} \exp[-1.03 (T_{1/3})_0 f^{-1}] \phi(\omega_h) \tag{11}$$

$$D(f, \theta) = \frac{2^{2s-1} \Gamma^2(s+1)}{\pi \Gamma(2s+1)} \cos^{2s} \left(\frac{\theta - \theta_0}{2} \right)$$

where S is the energy concentration factor, θ_0 the principal wave direction, Γ the Gamma function, and subscript '0' indicates the wave conditions in deep water. The input frequency spectrum is modified by the introduction of the shallow water effect. Consequently, significant wave height and wave period in deep water $((H_{1/3})_0, (T_{1/3})_0)$ are different from those at the offshore boundary of the computation region located in shallow water $((H_{1/3})_M, (T_{1/3})_M)$. In most cases, it is not $(H_{1/3})_0$ and $(T_{1/3})_0$ but $(H_{1/3})_M$ and $(T_{1/3})_M$ that are prescribed beforehand in the computation. The values of $(H_{1/3})_0$ and $(T_{1/3})_0$ to be given as input conditions are determined in a trial and error manner so that $(H_{1/3})_M$ and $(T_{1/3})_M$ computed from Eq.(11) agree approximately with the prescribed $(H_{1/3})_M$ and $(T_{1/3})_M$.

Numerical computation is conducted making use of a piecewise ray method as shown in Fig. 1. The method is to trace a wave ray backward only by one time step and to interpolate wave action spectral density at the tip point of the ray. The wave ray is followed by solving Eq. (3) and Eq. (4) with the Runge-Kutta method. In the ray computation, both input wave direction and current direction have to be reversed. The interpolation is executed in two steps. First, the Lagrange interpolation formula with third order accuracy is applied to the wave action spectral densities at the grid points surrounding the ray point in order to estimate the wave action spectral densities for the prescribed input directions, putting the wave direction at the ray point between them. It is given as

$$\omega_{i+r, j+s} = \sum_{i=i-1}^{i+2} \sum_{j=j-1}^{j+2} \left(\prod_{k=i}^{k=i-1} \frac{x-x_k}{x_1-x_k} \right) \left(\prod_{k=j}^{k=j-1} \frac{y-y_k}{y_1-y_k} \right) \omega_{ij} \tag{12}$$

$$r = (x - [x]) / \Delta x, \quad s = (y - [y]) / \Delta y$$

Second, the wave action spectral density for wave direction at the ray point is obtained by applying a linear interpolation on wave direction to the action densities estimated above.

$$w(f, \theta_m) = w(f, \theta) = w(f, \theta_k) + |w(f, \theta_{k+1}) - w(f, \theta_k)| \cdot \left(\frac{\theta - \theta_k}{\theta_{k+1} - \theta_k} \right) \tag{13}$$

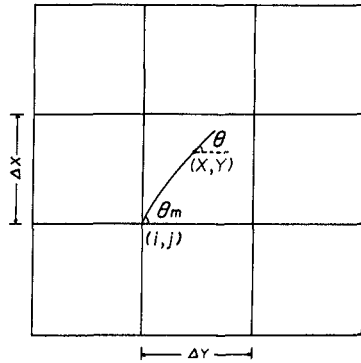


Fig. 1 Computation of direction of propagation.

(2) Nearshore current model

The equations used in the computation of nearshore currents are vertically-integrated continuity and momentum equations and they are expressed as

$$\begin{aligned} \frac{\partial \rho D}{\partial t} + \frac{\partial M_x}{\partial x} + \frac{\partial M_y}{\partial y} &= 0 \\ \frac{\partial M_x}{\partial t} + \frac{\partial}{\partial x}(UM_x) + \frac{\partial}{\partial y}(UM_y) &= -\rho g D \frac{\partial \eta}{\partial x} + \frac{\partial}{\partial x}(\bar{L}D \frac{\partial U}{\partial x}) + \frac{\partial}{\partial y}(\bar{L}D \frac{\partial U}{\partial y}) \\ &\quad - \left(\frac{\partial S_{xx}}{\partial x} + \frac{\partial S_{xy}}{\partial y} + \tau_{bx} \right) \\ \frac{\partial M_y}{\partial t} + \frac{\partial}{\partial x}(VM_x) + \frac{\partial}{\partial y}(VM_y) &= -\rho g D \frac{\partial \eta}{\partial y} + \frac{\partial}{\partial x}(\bar{L}D \frac{\partial V}{\partial x}) + \frac{\partial}{\partial y}(\bar{L}D \frac{\partial V}{\partial y}) \\ &\quad - \left(\frac{\partial S_{yx}}{\partial x} + \frac{\partial S_{yy}}{\partial y} + \tau_{by} \right) \end{aligned} \tag{14}$$

where $M_x = \rho DU$ and $M_y = \rho DV$.

The Longuet-Higgins expression (1970) is used as the lateral mixing term

$$\bar{L} = N_c \rho l_x \sqrt{gD} \tag{15}$$

where l_x is the distance measured from the real shoreline and $N_c (=0.01)$ the constant. The bottom friction components (τ_{bx}, τ_{by}) are obtained with Nishimura's expression (1983) for regular waves, which approximates the usual quadratic formula with high accuracy

$$\begin{aligned} \tau_{bx} &= \rho c_f \left\{ \left(w + \frac{\bar{u}^2}{w} \cos^2 \theta \right) U + \frac{\bar{u}^2}{w} \sin \theta \cos \theta V \right\} \\ \tau_{by} &= \rho c_f \left\{ \frac{\bar{u}^2}{w} \sin \theta \cos \theta U + \left(w + \frac{\bar{u}^2}{w} \sin^2 \theta \right) V \right\} \\ w &= \left(\sqrt{U^2 + V^2 + \bar{u}^2 + 2W\bar{u}} + \sqrt{U^2 + V^2 + \bar{u}^2 - 2W\bar{u}} \right) / 2 \\ W &= U \cos \theta + V \sin \theta, \quad \bar{u} = 2u_{max} / \pi, \quad u_{max} = \pi H / T \sinh kd \end{aligned} \tag{16}$$

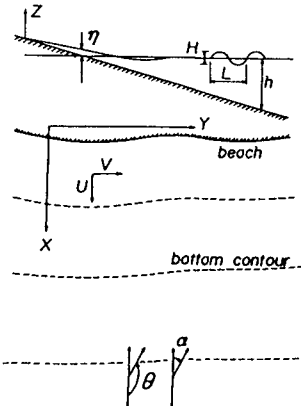


Fig. 2 Coordinate system used in nearshore current model.

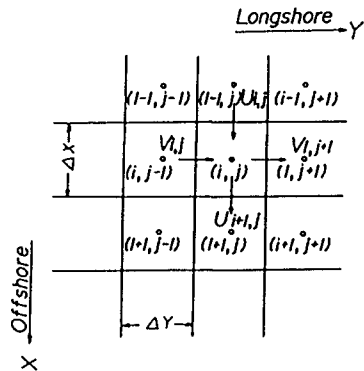


Fig. 3 Configurations of variables in finite difference model.

because their expressions in the case of irregular waves are not known by the author at least, where $c_f (=0.01)$ is the friction factor. The wave-induced velocity is estimated approximately by the small amplitude wave theory using H_{rms} , T_{m01} and $\bar{\theta}$ computed from the wave transformation model.

A finite difference method is used to solve the governing equations of nearshore currents. Fig. 2 is the coordinate system. The x and y axes are taken in the offshore direction, and in the longshore direction respectively and the z axis is taken vertically upward. Finite difference approximation is made by the forward difference in time and by the central difference in space under the configuration of variables shown in Fig. 3. Zero initial condition, fixed offshore and moving onshore boundary conditions, and periodic longshore boundary conditions are imposed respectively.

(3) Flow of computation

The computer program starts by determining the spatial distribution of wave characteristics under the given input conditions of offshore waves and bottom topography, and then nearshore current computation is made using the radiation stress components obtained from the wave transformation model.

A steady state solution is accomplished for 1000 to 2400 iterations of alternating computations of wave transformation and nearshore currents. In this case, computation of wave characteristics is executed every 18 iterations of nearshore current computation in order to save computer processing time. A schematic diagram of computation flow is shown in Fig. 4.

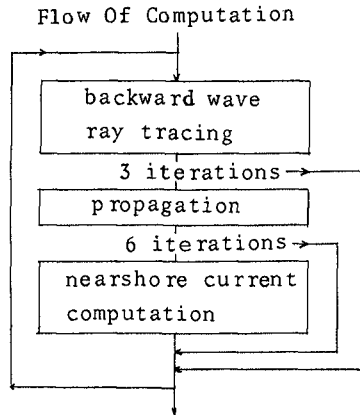


Fig. 4 Schematic diagram of computation flow.

Table 1 describes numerical conditions used in the computations of this study. Numbers of frequency segments and directional segments are 14 and 19 respectively.

3. EXPERIMENTAL AND OBSERVATIONAL VERIFICATIONS OF THE MODEL

(1) Comparison with experiments

A preliminary test in a smaller computational region was tried in order to tune the wave transformation model. Fig. 5 is a comparison between the computations and the experiments on wave height variation with normal incidence of waves on a uniformly sloping beach conducted by Battes and Janssen (1978). In order to approximate long-crested incident waves generated in the experiment, the value of 800 is used for

Table 1 Conditions used in the computations.

Model topography	Num. of grid MxN	Grid dist. (m)	$(H_{1/3})_0$ (m)	$(T_{1/3})_0$ (s)	$(H_{1/3})_M$ (m)	$(T_{1/3})_M$ (s)	α_M (°)	S	Num. of iterations
S. B.	24x8	1	0.304	2.15	0.204	1.74	0	800	1000
S. B.	45x8	1	0.304	2.15	0.204	1.74	0	800	2400
S. B.	45x8	1	0.221	2.25	0.147	1.81	0	800	2400
S. B.	23x8	12.5	1.30	4.20	1.00	3.54	30	20	1000
S. B.	23x8	12.5	1.30	4.20	1.00	3.54	30	800	1000
SY. C.	27x20	5	1.41	4.28	1.00	3.51	0	20	1000
ASY. C.	27x20	5	1.41	4.28	1.00	3.51	30	20	1000
SY. V.	27x20	20	2.06	3.95	2.00	3.66	0	20	1200
SY. V.	24x35	20	2.06	3.95	2.00	3.66	30	20	1200
C. B.	24x73	20	2.18	3.95	2.00	3.56	-20	20	1080
Sonu	19x26	5	0.586	5.00	0.300	3.77	0	40	1000

S. B.: straight beach, SY. C.: symmetrical concave topography, ASY. C.: asymmetrical concave topography, SY. V.: symmetrical convex shoreline, C. B. : arbitrarily curved bay, Sonu : bottom topography in Sonu's observation

the energy concentration factor in the directional spectral model and the direction data is taken to range from $162^\circ - 198^\circ$. The computation in the surf zone results in slightly greater value than the experiment. Thus, a correction to the saturated frequency spectrum in shallow water being used for the estimation of energy dissipation due to wave breaking is introduced to improve the correspondence with the experiment. The correction factor is determined as

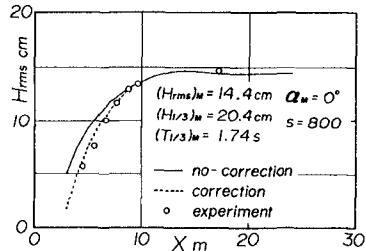


Fig. 5 Tuning of wave transformation model.

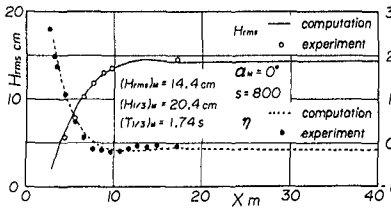


Fig. 6 Comparison of computed and measured wave heights and mean water level variations on a uniformly sloping beach.

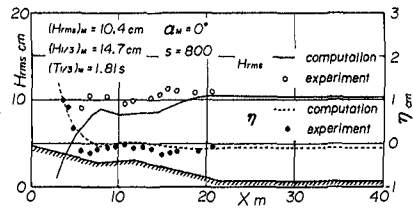


Fig. 7 Comparison of computed and measured wave heights and mean water level variations on a uniformly sloping beach with long-shore bar.

$$\beta = \begin{cases} -0.0471 \log^2 \left((H_{rms})_w / D \right) - 0.206 \log \left((H_{rms})_w / D \right) \\ -0.875; (H_{rms})_w / D > 0.484 \\ 1; (H_{rms})_w / D \leq 0.484 \end{cases} \quad (17)$$

Cross-shore distributions of wave height and mean water level variation computed in a larger computational region for the same case are re-compared with the experiment in Fig. 6. As a matter of course, the computation of wave height variation is in good agreement with the experiment. Consequently, the computation of mean water level variation also shows good correspondence with the experiment.

Fig. 7 is another comparison between the computation and the experiment by Battjes and Janssen on a uniformly sloping beach with a longshore bar. The agreement of wave height variation is not always satisfactory compared to that of wave set-up and set-down, because energy dissipation due to wave breaking is not well-formulated in the present model.

(2) Comparison with observation

Fig. 8 illustrates the observed nearshore current patterns by Sonu (1972) and the corresponding results computed by the present model. The model reproduces well the qualitative features of the complicated nearshore current patterns found in the observation, such as the onshore currents on both sides of the region and the rip currents in the central part. But, in a quantitative sense, outflow from the rip channel in the computation seems to be a little stronger than that in the observation.

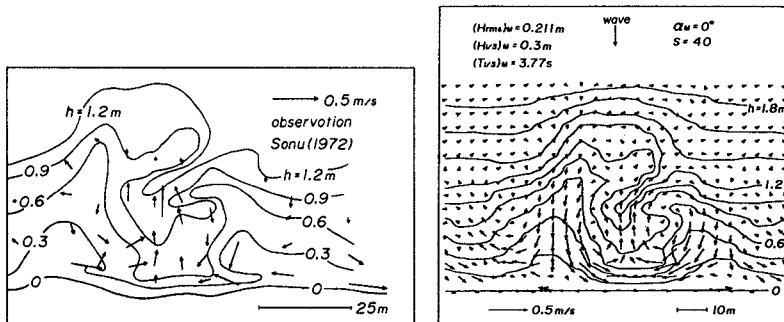


Fig. 8 Nearshore current patterns observed by Sonu(1972) and the corresponding results computed by the present model.

4. COMPUTATIONAL RESULTS AND CONSIDERATIONS

(1) Computations on model topographies

The model is applied to the nearshore current computations on a uniformly sloping beach and on model topographies with two-dimensional variation of bottom contour. The computations are compared with those based on regular wave

theory (Yamaguchi et al. 1983 and 1985) and the effect of wave irregularity on wave transformation and nearshore currents is discussed.

(2) Uniformly sloping beach

The cross-shore distributions of wave height, wave direction, mean water level variation and longshore current profile on a plain beach with a slope of 0.016 are drawn in Fig. 9. In the case of irregular waves, the computations using energy concentration factor $S = 20$ or 800 or neglecting the wave-current interaction are carried out. The effect of wave-current interaction is weak in this case and the effect of the energy concentration factor appears distinctly in longshore current velocity. Compared to the case of regular waves, the variations of wave height and wave direction in the surf zone and in shoaling water is slower. As a result, offshore variations of the resulting radiation stress, wave set-up and set-down and longshore current velocity have a similar tendency, and the magnitudes of mean water level variation and longshore current velocities become smaller.

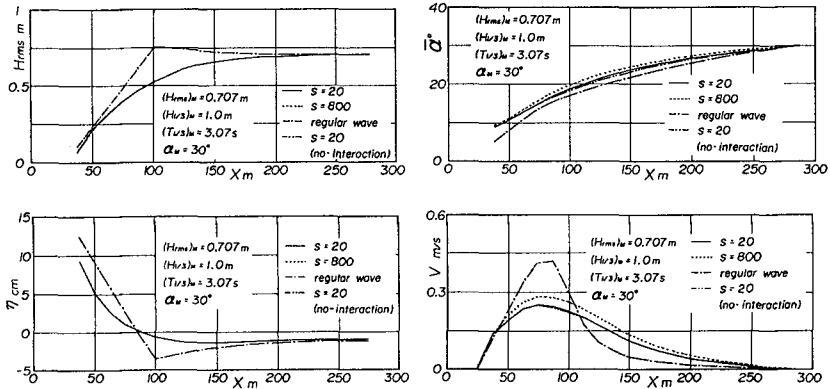


Fig. 9 Cross-shore distributions of wave height, wave direction, mean water level variation and longshore currents on a uniformly sloping beach.

(3) Bottom topography with a concave contour line

The bottom topography model proposed by Noda (1974) is first chosen for the computation of nearshore currents on a two-dimensional topography and it is expressed as

$$h(x, y) = ix [1 + A_0 \exp\{-3(x/20)^{1/2}\} \sin^{10}\{(\pi/\lambda)(y - x \tan \epsilon)\}] \quad (18)$$

where i is a mean beach slope of 0.025, λ the longshore beach length of 80 m, A_0 the maximum amplitude of the bottom undulation of 20 m and ϵ the skewness of the bottom undulation of 0° or 30° . The model topographies with $\epsilon = 0^\circ$ and with $\epsilon = 30^\circ$ are referred to as symmetrical concave topography and asymmetrical concave topography respectively.

Fig. 10 show the nearshore current patterns with normal

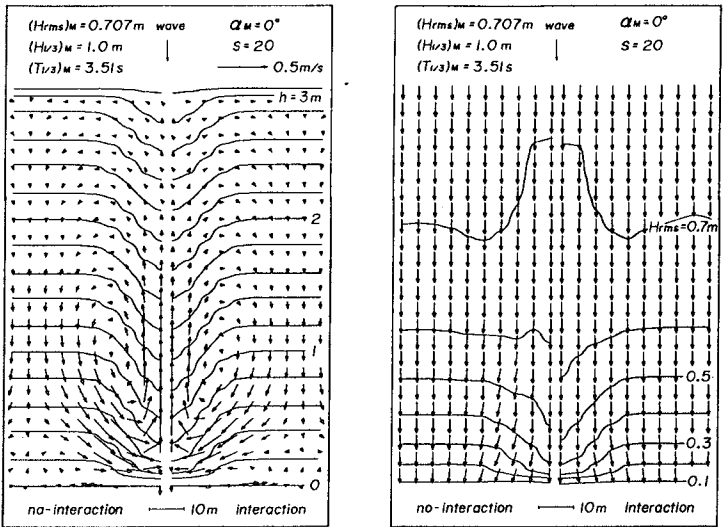


Fig. 10 Effect of wave-current interaction on nearshore currents, wave height and wave direction on a symmetrical concave topography.

incidence of waves on the symmetrical concave topography. The case neglecting wave-current interaction is on the left hand side and the normal case is on the right hand side. We can see the formation of a pair of seaward nearshore current cells and a pair of weak and flat cells near the shoreline, and the neglect of wave-current interaction increases cross-shore current velocity such as in the case of regular waves.

Fig. 11 illustrates the current patterns with oblique incidence of waves on the asymmetrical concave topography. Meandering longshore currents are predominant, but a small and flat circulation cell in the region with concave contour line near the shore is also found.

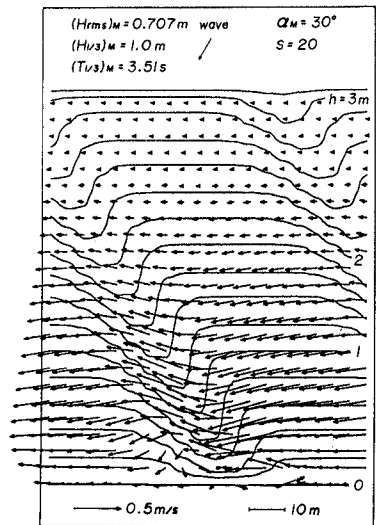


Fig. 11 Nearshore current patterns on asymmetrical concave topography.

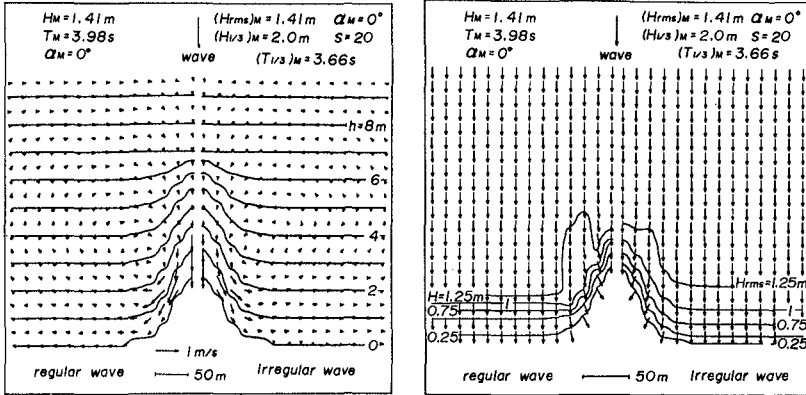


Fig. 12 Effect of wave irregularity on nearshore currents, wave height and wave direction on a model topography with convex shoreline.

(4) Bottom topography with a convex shoreline

Fig. 12 show the spatial distributions of wave height and wave direction, and the corresponding nearshore current patterns on a two-dimensional model topography with convex shoreline. On the left hand side of each figure, the results based on a regular wave theory are given as well. In the computations, root mean wave height and peak period of frequency spectrum and principal wave direction are used as input conditions. In each case, a pair of nearshore current cells with rotational direction contrary to the case of symmetrical concave topography mentioned above are formed and on the center line of the computational region, the onshore current is accelerated toward the shoreline and the current direction turns to be tangential to the contour line. Current patterns in both cases are very similar to each other, but current velocity in the case of irregular waves is smaller by about 30 %.

Fig. 13 is the current pattern in the case of obliquely incident waves. Predominant longshore currents develop along the contour line and a weak counterclockwise circulation cell appears near the shoreline in the upwave region.

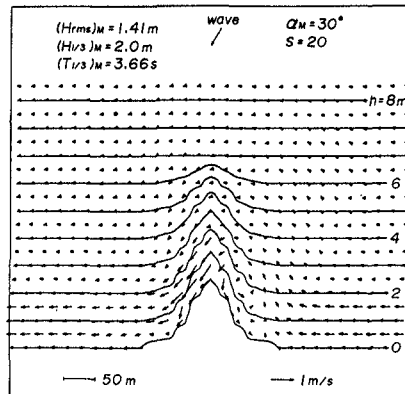


Fig. 13 Nearshore current patterns on a model topography with convex shoreline.

(5) Bottom topography with an arbitrarily curved shoreline

Nearshore current patterns on a curved bay computed by regular and irregular wave models are shown in Fig. 14. Both these figures demonstrate the predominant longshore currents in the outer region and a clockwise nearshore circulation cell in the inner region. This cell exists irrespective of incident wave direction. But, a weak offshore circulation cell found in the case of regular waves disappears in the case of irregular wave case.

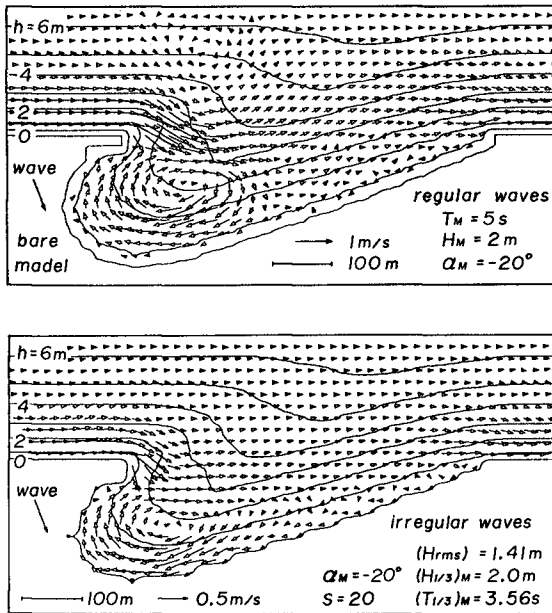


Fig. 14 Spatial distribution of nearshore current patterns on a curved bay computed by the numerical models with regular and irregular wave theories.

5. CONCLUSIONS

A numerical model of nearshore currents induced by irregular waves was proposed and its validity was supported by reasonable correspondence with experimental and observational results. Moreover, the effect of wave irregularity was considered, based on numerical computations. Comparison with the results based on a regular wave model shows that wave irregularity has a smoothing effect on cross-shore distribution of wave height, mean water level variation and longshore currents, but that it does not have much effect on nearshore current patterns.

6. ACKNOWLEDGMENTS

Thanks are due to Messrs. K. Hosono and H. Kawahara, former graduate course students of Ocean Engineering, Ehime University, for their valuable help during the study. A part of this study was accomplished with the support of the Science Research Fund of the Ministry of Education, for which the author expresses his appreciation.

REFERENCES

- Battjes, J.A. (1972): Set-up due to irregular waves, Proc. of 13th ICCE, Vol. III, pp. 1993 - 2004.
- Battjes, J.A. and J.P.F.M. Janssen (1978): Energy loss and set-up due to breaking of random waves, Proc. of 16th ICCE, Vol. I, pp.569 - 589.
- Collins, J.I. (1972): Longshore currents and wave statistics in the surf zone, Rep. No. TC-149-2, Tetra Tech. Inc.
- Hubertz, J.M. (1984): Modeling of nearshore driven currents, Proc. of 19th ICCE, Vol. III, pp. 2208 - 2219.
- Kitaigorodskii, S.A. et al. (1975): On Phillips' equilibrium range in the spectra of wind generated gravity waves, Jour. Phys. Oceanogr., Vol. 5, pp. 410 - 420.
- Longuet-Higgins, M.S. (1970): Longshore currents generated by obliquely incident sea waves Part 2, Jour. Geophys. Res., Vol. 75, No. 33, pp. 6778 - 6801.
- Nishimura, H. (1982): Numerical simulation of nearshore circulation, Proc. of 29th Conf. on Coastal Eng. in Japan, pp. 333 - 337 (in Japanese).
- Noda, E. (1974): Wave-induced nearshore circulation, Jour. Geophys. Res., Vol. 79, No. 27, pp. 4097 - 4106.
- Sonu, C.J. (1972): Field observation of nearshore circulation and meandering currents, Jour. Geophys. Res., Vol. 77, No. 8, pp. 3232 - 3246.
- Thornton, E.B. and R.T. Guza (1986): Surf zone longshore currents and random waves: Field data and models, Jour. Geophys. Res., Vol. 16, pp. 1165 - 1179.
- Yamaguchi, M. et al. (1983): A numerical solution of near-shore currents taking account of wave-induced mass flux, Proc. of 30th Conf. on Coastal Eng. in Japan, pp. 480 - 484 (in Japanese).
- Yamaguchi, M. et al. (1985): A numerical model of nearshore currents applicable to coastal area with an arbitrarily curved shoreline, Proc. of 32nd Conf. on Coastal Eng. in Japan, pp. 248 - 252 (in Japanese).

Yamaguchi, M. (1986): A numerical model of nearshore currents based on a finite amplitude wave theory, Proc. of 20th ICCE, Vol. 1, pp. 849 - 863.